数理解析研究所講究録 1406 巻 2004 年 108-118

Wavelets & Turbulent Flow. Some Aspects of Data Analysis

Markus Uhlmann
Dept. Combustibles Fósiles
CIEMAT
Avenida Complutense 22, 28040 Madrid, Spain
markus.uhlmann@ciemat.es

Jochen Fröhlich
Institut für Chemische Technik
Universität Karlsruhe (TH)
Kaiserstrasse 12, 76128 Karlsruhe, Germany
froehlich@ict.uni-karslruhe.de

May 26, 2004

1 Abstract

We discuss a discrete orthogonal wavelet basis which fulfills the requisites for the analysis of flow data in bounded domains. Definitions of the scale and position attributes are given for the modes which are not translationally invariant in this case. Visualization techniques are discussed and demonstrated for analytical data. As an application, wall-normal local wavelet spectra are computed from statistical data of turbulent plane channel flow at low Reynolds number. The results show a linear increase of the most energetic scales with wall-distance for all velocity components.

2 Introduction

In the past, investigations of the dynamics of turbulent flows have often focused upon the role which significant length scales play in the process under consideration (e.g. non-linear energy transfer). When taking the point of view of Fourier space analysis, the scale corresponds to the wavelength of a global mode. On the other hand, it has long been recognized that coherent structures are responsible for numerous experimentally and numerically observed phenomena in turbulent flow (Jeong et al., 1997). Clearly, the non-local approach is not optimal for capturing a localized feature with a small number of modes.

When dealing with statistics of turbulent flow fields, proper orthogonal decomposition (POD) can be used to extract the most energetic modes (e.g. Liu et al., 2001). However, no clear-cut *a priori* definition for physical scales and their positions is available in the framework of the POD formalism.

It is an appealing feature of wavelet analysis that it does provide access to both scale and space information simultaneously and in a pre-determined fashion. In a growing number of studies since the early 1990's, the wavelet formalism has been applied to turbulent flow data as reviewed by Farge et al. (1999). However, applications to the wall-normal direction of confined flows (channels, boundary layers, pipes, etc.) have not yet appeared in the literature. This gap is probably due to the lack of suitable wavelet functions tailored for their use on the interval – as opposed to most of the classical constructions which apply to the real line or the torus.

By "suitable" – for the purpose of flow analysis – we mean that wavelet functions should satisfy the following general requirements:

(i) Wavelets form a discrete-orthogonal basis. Such a transform is non-redundant and conserves the data volume (Meneveau, 1991), a critical issue as data sets of turbulent flows typically are extremely large.

(ii) Orthogonality holds for a scalar product with a weight of unity. This allows to link wavelet coefficients directly to a mode's contribution to the total energy, as in Fourier analysis (Parseval's theorem).

(iii) The basis possesses fundamental symmetry properties. These ensure that the analysis does not break possible symmetries of the data.

(iv) Wavelet functions are reasonably localized in physical space and scale space. This property is vital for a meaningful definition of position and scale attributes.

Existing wavelet functions do not seem to match these criteria. In particular, Daubechies wavelets are not symmetric and become highly irregular near the boundary of the interval (Cohen et al., 1994). Techniques where the interval is mapped to a periodic space, as proposed by Maday and Ravel (1992), lead to a basis which violates (ii).

Fröhlich and Uhlmann (2002) introduced a construction based upon Legendre polynomials leading to a wavelet basis which complies with conditions (i)-(iii) above, but which fulfills (iv) only marginally since the functions have a poor localization in space with an asymptotic decay of only x^{-1}.

Recently, Fröhlich et al. (2003) used a systematic approach for the construction of wavelets based on orthogonal functions leading to a new basis with improved spatial localization. The purpose of the present paper is to apply this new basis to data from direct numerical simulation (DNS) of turbulent plane channel flow and thereby to improve upon earlier results obtained by means of the previous (less-well localized) basis used in Uhlmann and Fröhlich (2002).

The remainder of this paper is organized as follows. First we specify the new wavelet basis, its shape and spatial decay. Then we discuss how position and scale attributes can be defined in the case of a bounded domain, before moving on to the problem of visual presentation of wavelet coefficients. We go on exposing the properties of the transform by means of analytic data before finally turning to turbulent channel flow and the presentation of local power spectra.

3 Localized Legendre wavelets

Fröhlich et al. (2003) use a Malvar-type construction (Malvar, 1990) for lumping together smoothly-varying bands of orthogonal polynomials in order to control the spatial localization. Wavelets ψ_{ji} and scaling functions φ_{ji} with scale index j and shift index i are then defined as:

$$\left.\begin{aligned} \psi_{ji}(x) &= \sum_{k=1}^{\infty} w_j(k)\, b_{ji}(k)\, P_k(x) \\ \varphi_{ji}(x) &= \sum_{k=1}^{\infty} \tilde{w}_j(k)\, \tilde{b}_{ji}(k)\, P_k(x) \end{aligned}\right\} \quad \begin{aligned} &j \in \mathrm{N}_0 \\ &i = 0, \ldots, 2^j - 1 \end{aligned} \tag{1}$$

where $P_k(x) \equiv \sqrt{k+1/2}L_k(x)$ with $L_k(x)$ the standard Legendre polynomial. The coefficients are defined as:

$$\begin{aligned} \tilde{b}_{ijk} &= \frac{1}{\sqrt{1+\delta_{k,k_{-1}}}}\sqrt{\frac{2}{\tilde{K}_j}}\cos\left(\pi\frac{k-k_{-1}}{\tilde{K}_j}(i+1/2)\right) \\ b_{ijk} &= (-1)^{i+1}\sqrt{\frac{2}{K_j}}\cos\left(\pi\frac{k-k_j}{K_j}(i+1/2)\right) \end{aligned} \tag{2}$$

and the window functions as

$$w_j(k) = \begin{cases} g_{db}\left(\frac{k-k_j}{\Delta k_j}\right) & \begin{cases} k_j - \Delta k_j < k < k_j + \Delta k_j \\ \wedge \quad \Delta k_j > 0 \end{cases} \\ 1 & \begin{cases} k_j + \Delta k_j \leq k \\ \wedge \quad k < k_{j+1} - \Delta k_{j+1} \end{cases} \\ g_{db}\left(-\frac{k-k_{j+1}}{\Delta k_{j+1}}\right) & \begin{cases} k_{j+1} - \Delta k_{j+1} < k \\ \wedge \quad k < k_{j+1} + \Delta k_{j+1} \\ \wedge \quad \Delta k_j > 0 \end{cases} \\ 0 & \text{else} \end{cases} \tag{3}$$

$$\tilde{w}_j(k) = \sqrt{\sum_{l=-1}^{j-1} w_l^2(k)}$$

The widths of the windows are chosen in a dyadic fashion as

$$k_j = \begin{cases} 0 & j = -1 \\ 2^j & \text{else} \end{cases}, \Delta k_j = \begin{cases} 0 & j = -1 \\ \frac{1}{3} K_j & \text{else} \end{cases} \tag{4}$$

with

$$K_j = k_{j+1} - k_j\,, \quad \tilde{K}_j = k_j - k_{-1} \tag{5}$$

Finally, the smoothing function selected is the one suggested by Daubechies (1992), viz.

$$\begin{aligned} g_{db}(\xi) &= \sin\left(\frac{\pi}{2}\nu\left(\frac{1+\xi}{2}\right)\right) \\ \nu(x) &= x^4(35 - 84x + 70x^2 - 20x^3) \end{aligned} \tag{6}$$

The basis functions (1) possess the necessary orthogonality properties and allow for a decomposition of square integrable functions as:

$$u(x) = c_{00}\varphi_{00}(x) + \sum_{j=0}^{\infty}\sum_{i=0}^{2^j-1} d_{ji}\psi_{ji}(x)\,, \quad x \in [-1, 1] \tag{7}$$

where the coefficients of the transform c_{00}, d_{ji} are obtained from the scalar product between the signal and the corresponding basis functions. It should be noted that the numerical algorithm (with the upper bound for j finite in (7)) boils down to performing a Legendre transform of the data and then computing a linear combination of the Legendre coefficients. The total energy of the signal is simply expressed by the sum of the square of all coefficients:

$$\int_{-1}^{+1} u^2(x)\,\mathrm{d}x = c_{00}^2 + \sum_{j,i} d_{ji}^2 \tag{8}$$

4 Definition of physical attributes

Figure 1 shows the shape of the present wavelet functions with scale index $j = 5$ for a central position in the interval and close to the boundary. The spatial decay is x^{-5} for wavelets located away from the boundaries and for large j (cf. figure 2). This is a considerable improvement over the basis of Fröhlich and Uhlmann (2002) which is clearly visible in the graph. Additionally,

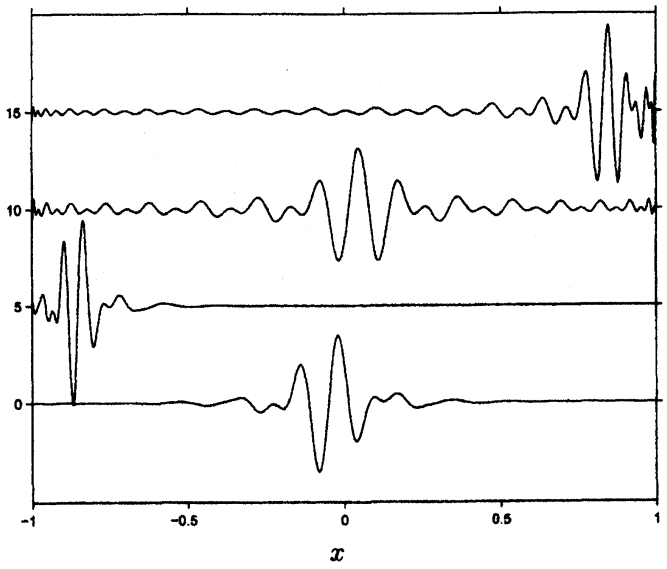

Figure 1: Wavelet functions $\psi_{ji}(x)$ with scale index $j = 5$ and position indices $i = 15, 5, 16, 26$ from bottom to top. The lower two curves correspond to the present basis, while the upper two are the wavelets of Fröhlich and Uhlmann (2002).

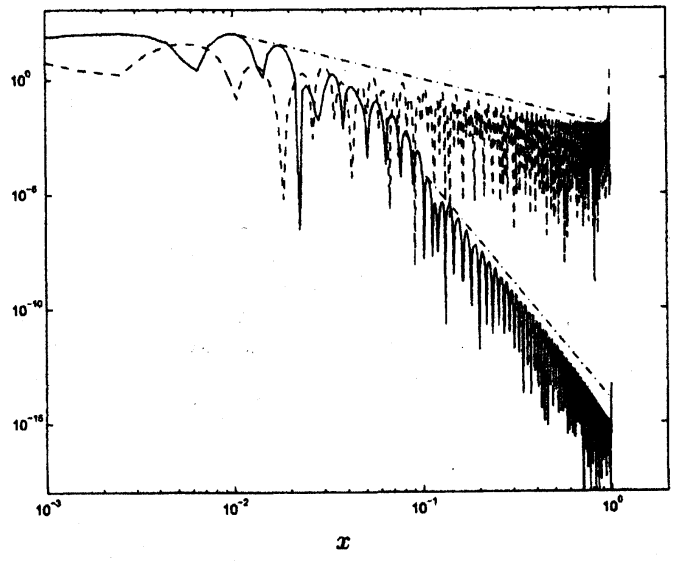

Figure 2: Decay of the square of the wavelet functions $\psi_{ji}^2(x)$ with scale index $j = 8$ and position index $i = 128$. The lower curve corresponds to the present basis, the upper one to the basis of Fröhlich and Uhlmann (2002). The straight reference lines are proportional to x^{-10} and x^{-2}, respectively.

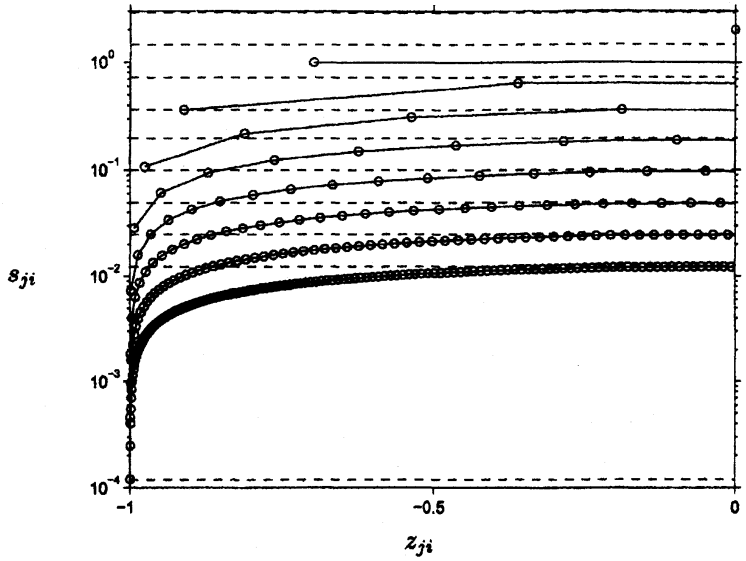

Figure 3: Semi-logarithmic plot of scale s_{ji} versus position z_{ji} for a basis with $j \leq 8$. Data points for a constant scale index j are connected by solid lines. The dashed lines indicate the chosen values for the bins used in the definition of the global wavelet spectrum (12). Please note that only half of the interval is shown.

the present basis functions are free from spurious "tails" which were observed in (Fröhlich and Uhlmann, 2002) near the bounds of the interval, even for centrally located wavelets.

The present approach follows the multi-resolution idea of Mallat (1989) quite closely and yields a relatively simple construction. Due to the uneven spacing of the zeros of the Legendre polynomials, however, Legendre-based wavelet functions are no longer invariant under translation and scaling in the usual linear way. Hence, the definitions of "position" and "scale", which can then be attributed to particular modes, need to be adapted to this situation when the decomposition (7) is to be interpreted in physical terms.

4.1 Position

While in the case of translation-invariant functions the position is simply proportional to the shift index i, we need to consider the shape of the wavelets in the present case. The functions $\psi_{ji}(x)$ given by (1) are "odd" in the sense defined by Fröhlich et al. (2003). Consequently, we define their center positions z_{ji} as the zero-crossings enclosed by the two largest local extrema with opposite sign. The values for z_{ji} are not available in closed form, but can be obtained by a fixed-point iteration (a good initial guess is the ith zero of the Chebyshev polynomial of the second kind of degree j).

4.2 Scale

The definition of the notion "scale" also requires revisiting in the present framework. By analogy with the periodic case or the real line one could define the scale-number of a particular wavelet $\psi_{ji}(x)$ via the polynomial degrees retained in the respective window $w_j(k)$, e.g. we might take the center of the window $(k_{j+1} + k_j)/2$. The inverse of this quantity, multiplied by the length of the interval, gives a length scale. However, such a definition is not very useful since a polynomial degree alone does not correspond to a single wave-number in the Fourier sense. This becomes immediately clear if we consider how the oscillations of a Legendre polynomial are "squeezed" close to the boundary of the interval; the same effect can be observed when comparing the two

lower graphs in figure 1, bearing in mind that wavelets with common scale index j have identical window functions $w_j(k)$.

As an alternative we propose to define the scale s_{ji} directly from the center positions z_{ji} by taking the distance between neighboring mid-points:

$$s_{ji} = Z_{ji} - Z_{j(i-1)} \tag{9}$$

More specifically, the mid-points are defined as:

$$Z_{ji} = \begin{cases} -1 & i = 0 \\ +1 & i = 2^j - 1 \\ \dfrac{z_{j(i+1)} + z_{ji}}{2} & \text{else} \end{cases} \tag{10}$$

For the present basis, this definition yields a progressive decrease of scale when approaching one of the interval's boundaries (while keeping the index j constant), very similar to the grid-spacing of a Legendre-Gauss-Lobatto grid (cf. figure 3). Thereby, it reflects the observed change in characteristic frequency of oscillation of the wavelet functions near the end-points. Please note that the definition (9) is consistent with the standard case: setting $\tilde{z}_{ji} = -1 + 2^{-j} + i\,2^{1-j}$ and substitution into (9) leads to $\tilde{s}_{ji} = 2^{1-j}$, i.e. dyadic dilations independent of the shift index.

5 Visual presentation by means of the scalogram

5.1 Definition of the scalogram

An important point of the analysis is the appropriate visual representation of wavelet coefficients. The usual graph – called "scalogram" – shows a discrete two-dimensional arrangement of scale versus position, each cell being colored with grey-scales according to the absolute value of the respective coefficient. Here, we need to take into account the non-uniformity of the translation and dilation of the present wavelets when plotting results. Fröhlich and Uhlmann (2002) developed a method where – due to the above mentioned similarity between the exact centers z_{ji} and the roots of the Chebyshev polynomials of the second kind – a continuous distortion of the classical scalogram is used to give a readable representation of the variation of scale with position (cf. figure 4 discussed below).

5.2 An analytical signal

The properties of the present wavelet basis are discussed in detail by Fröhlich et al. (2003). Here, we provide an illustration by means of a synthetic signal in form of a Gaussian bump

$$u(x) = \exp\left(-\frac{1}{2}\left(\frac{x - x_c}{\sigma}\right)^2\right) \tag{11}$$

It corresponds to a localized feature with a characteristic length scale σ and a well-defined center position x_c so that this signal is representative of a coherent structure with the respective position and scale in a real flow. Its transform is shown in form of a scalogram in figure 4 for $\sigma = 0.01$ with $x_c = 0$ and $x_c = 0.9$. Scale and position of the bump can be determined in wavelet space approximately by selecting the most excited modes. It is a noteworthy feature of the present basis that this is still possible when the peak is located near the boundary, where strong end-effects appear when using a standard basis constructed for the real line or the torus.

The scalograms also show that the energy of the signal is carried by a relatively small number of modes (15 modes make up about 95% of the energy in the example) and, particularly, that a considerable part enters the ubiquitous $j = 0$-mode. This fact should be kept in mind when analyzing flow fields later on.

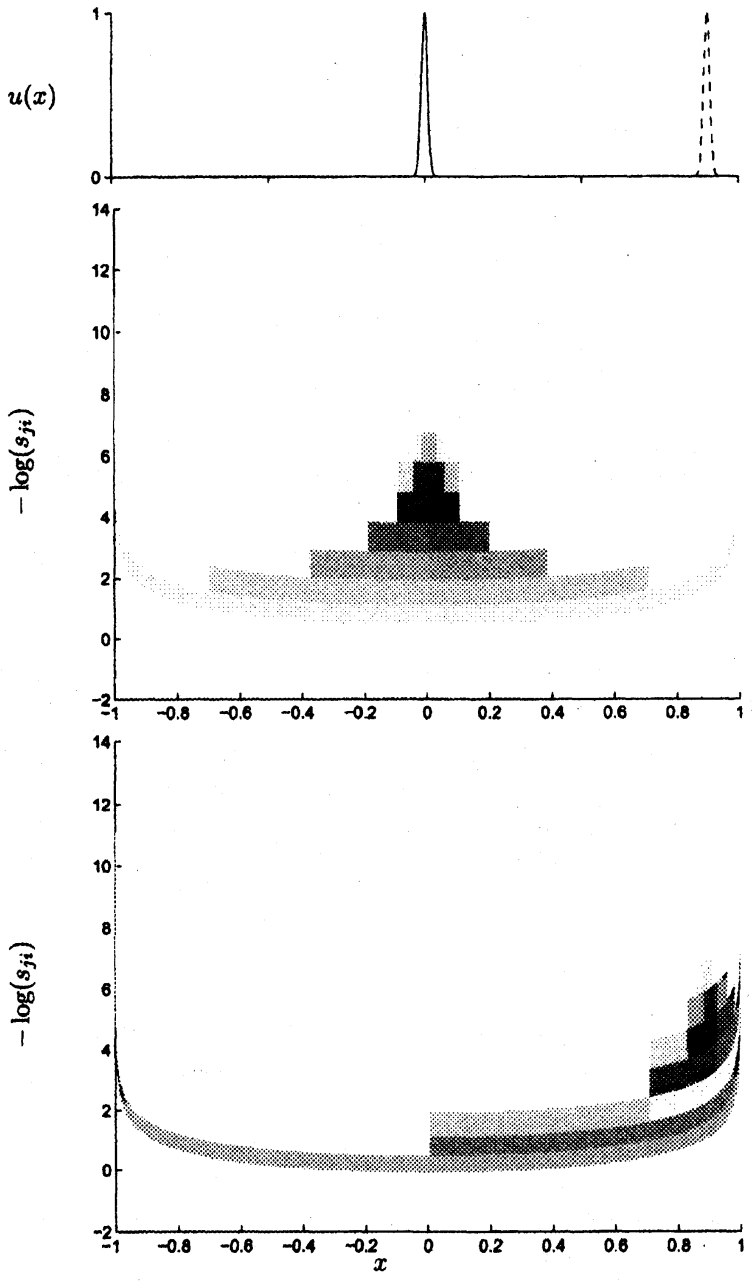

Figure 4: Coefficient scalogram of the transform of a Gaussian bump with center $x_c = 0$ (center) and $x_c = 0.9$ (bottom). In both cases, the standard deviation is $\sigma = 0.01$. The grey-scale varies linearly from white ($|d_{ji}| = 0$) to black ($|d_{ji}| = \max_{ji} |d_{ji}|$). The abscissa gives the position of the modes z_{ji}, the ordinate corresponds to $-\log_2(s_{ji})$, i.e. large scales are located near the bottom of the two graphs. The top graph shows the two signals $u(x)$ in physical space.

6 Visualization through wavelet-spectra

The scalogram gives a useful global view of the wavelet coefficients. For quantitative studies, however, power spectra are more appropriate. They are frequently used in Fourier analysis and have become an important diagnostic tool in wavelet analysis.

6.1 Global power spectrum

Let us define the global power-spectral density per unit wavenumber according to (Fröhlich and Uhlmann, 2002) as

$$E^{(g)}(k^{(m)}) = \frac{1}{\Delta k^{(m)}} \sum_{j,i/k^{(ji)} \in [k_L^{(m)}, k_R^{(m)}]} d_{ji}^2 \tag{12}$$

Here, a pseudo-wavenumber is defined as the inverse of the scale of a mode, i.e. $k^{(ji)} = 1/s_{ji}$. The range of wavenumbers is first partitioned into logarithmic intervals $[k_L^{(m)}, k_R^{(m)}]$ with band-width $\Delta k^{(m)} = k_R^{(m)} - k_L^{(m)}$ and associated characteristic wavenumber $k^{(m)} = \exp(\log((k_R^{(m)} + k_L^{(m)})/2))$. Presently selected bins are shown in figure 3 for a basis with $j \leq 8$. Then, squares of coefficients are summed if the wavenumber of the corresponding mode falls into the desired interval. Thereby, contributions from modes are selected irrespective of their center location.

6.2 Local power spectrum

Of particular interest is the local power-spectral density per unit wavenumber, defined in the present context as (Fröhlich and Uhlmann, 2002):

$$E(x,j) = 2^j \frac{d_{ji^*}^2}{\Delta k^{(ji^*)}} \tag{13}$$

The quantity $E(x,j)$ is evaluated at the location x and therefore for each scale index j, the mode for which the distance $|x - z_{ji}|$ takes a minimum is selected and denoted with the position index i^*. Hence, the local spectrum can be imagined as a vertical cut through a scalogram. The wavenumber band $\Delta k^{(ji^*)}$ is computed from the wavenumbers of all modes which enter the spectrum at the respective location. The factor 2^j was introduced by Do-Khac et al. (1994) in the context of a periodic basis for compatibility with the global spectrum which then simply becomes the average over all local spectra. In the present case, this statement is only true in an approximate sense and we maintain the rescaling factor in (13) such as to allow for a direct comparison between local and global spectra.

With the help of the quantity (13) it is now possible to analyze the distribution of energy by scales of motion for different locations in space. Subsequently, we will apply this technique to velocity signals recorded along the wall-normal direction of channel flow. Therefore, the argument x corresponds to a wall distance and the scale index j can be translated into a wall-normal length scale s_{ji^*} of a mode. All lengths will be given in non-dimensional wall units denoted by a superscript "+".

7 Turbulent plane channel flow

7.1 The flow case

The data was obtained by pseudo-spectral DNS of turbulent plane channel flow in a doubly-periodic box of streamwise and spanwise extent $2\pi h$ and πh, respectively, where h is half the separation of the walls. The discretization uses $600 \times (385) \times 600$ Fourier (Chebyshev) modes and the Reynolds number based upon wall-friction velocity is $Re_\tau = 590$. Statistics were accumulated from 5 instantaneous flow fields taken over one flow-through period, corresponding to 240 viscous time units (equivalently 9 outer flow time units).

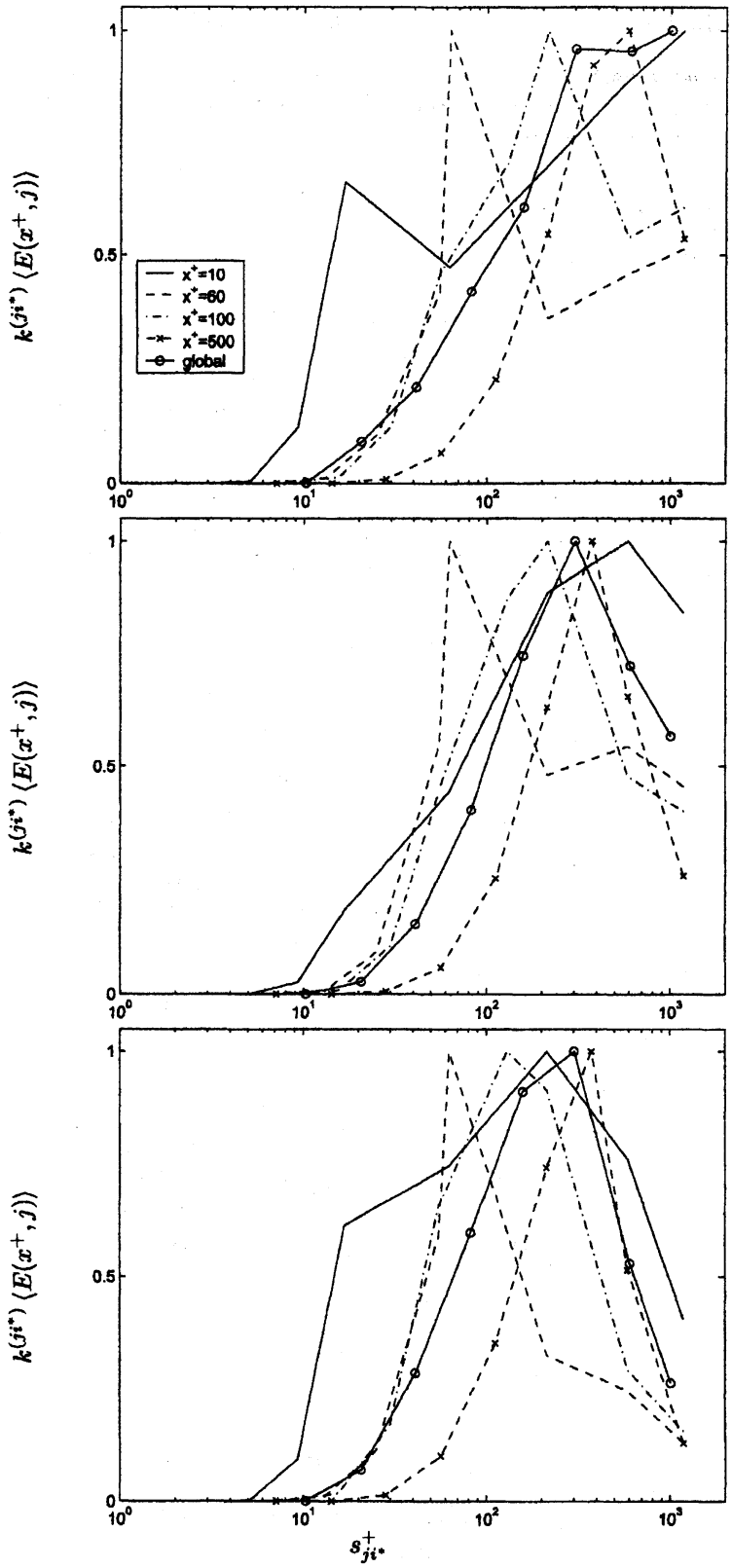

Figure 5: Global and local pre-multiplied power spectra obtained from statistics of the transform of velocity fluctuations recorded along the wall-normal direction in plane channel flow at $Re_\tau = 590$. Top: streamwise velocity component; center: wall-normal component; bottom: spanwise component. All curves are normalized by their maximum value.

7.2 Results

Figure (5) shows the pre-multiplied local spectra $k^{(ji^*)}\,\langle E(x^+,j)\rangle$, where $\langle\cdot\rangle$ stands for the average over the available samples. The three velocity components are transformed and analyzed separately. Please note that the mean velocity has been subtracted from the streamwise component. The global spectrum has been added for reference purposes. The curves are normalized by their maximum value with the purpose of emphasizing the frequency content. The scales are bounded from above by the channel height, $s^+_{ji^*} \leq 2Re_\tau$. For increasing wall distance, it can be observed that the small-scale end of the spectra is less excited, which means that the range of excited scales is becoming narrower when approaching the center of the channel.

All spectra have a tendency towards more pronounced local extrema as compared to the results of Uhlmann and Fröhlich (2002) who used the linearly-decaying basis of Fröhlich and Uhlmann (2002) on the same data. This observation confirms the superiority of the present basis which should be preferred in future studies.

From the above mentioned peaks one can determine a characteristic length-scale corresponding to the most energetic mode at a given location. Except for the near-wall region ($x^+ = 10$), the most-excited length-scale is roughly equal to the wall-distance. This implies that from the buffer-zone outwards, the energetic modes reach all the way down to the wall, as stated by Townsend's attached eddy hypothesis (Townsend, 1976).

The fact that the local spectrum evaluated at $x^+ = 10$ peaks at scales measuring $200 \ldots 1000$ wall units can be explained by the sparse character of discrete-orthogonal bases at large scales. Hereby the contributions of the largest modes fully enter even at remote locations. However, a local extremum at $s^+_{ji^*} \approx 15$ is visible for the streamwise component.

This brings us to the comparison of the energy distribution for the different Cartesian components of velocity. The observations above hold in a similar way for all the three components of the velocity vector. The main difference, apart from the local peak of streamwise velocity near the wall, lies in the decay at the large-scale end of the spectrum. At all locations (and for the global spectrum) the spanwise component has less than 50% of relative energy density contained in the largest scale, while for the streamwise component this value lies between 50-100%. Results for the wall-normal velocity component fall in between those two categories. Data from simulations with higher Reynolds numbers should be investigated in order to further clarify the decay properties for large scales. Furthermore, the accumulation of additional statistics for the present data set should be considered.

8 Conclusions

We have shown how signals on the interval can be decomposed by means of new Legendre wavelet functions. Desirable features of this discrete-orthogonal basis are the existence of an intuitive energy decomposition (8), its symmetry and the improved spatial localization with an asymptotic decay rate of x^{-5}. As a prize for using a Legendre basis, one has to relax the usual invariance of the functions under translation and rescaling when approaching the interval boundaries. For these conditions, we have provided adequate definitions for the position and scale attributes which allow to perform a non-classical multi-resolution analysis, as demonstrated by an analytical example.

For our analysis of statistical data from DNS of turbulent plane channel flow we have used local power spectra formulated for the present type of basis. The results show a linear increase of the most energetic wall-normal length scale with wall-distance in the logarithmic region of the flow and for all velocity components.

A possible future extension of the present work is the construction of a multi-dimensional basis and its application to planes or rectangular domains of flow data as performed in Fröhlich and Uhlmann (2002) for the earlier construction. A straightforward method advocated in this reference is the use of tensor product wavelets which even allows the selection of different basis functions in each coordinate direction.

Acknowledgements

JF gratefully acknowledges the support of SFB 606 at the University of Karlsruhe.

A. Cohen, I. Daubechies, and P. Vial. Wavelets on the interval and fast wavelet transform. *Appl. Comput. Harmonic Anal.*, 1:54–81, 1994.

I. Daubechies. *Ten lectures on wavelets.* CBMS-NSF Reg. Conf. Series Appl. Math. SIAM, Philadelphia (PA), USA, 1992.

M. Do-Khac, C. Basdevant, V. Perrier, and K. Dang-Tran. Wavelet analysis of 2d turbulent fields. *Physica D*, 76:252–277, 1994.

M. Farge, N. Kevlahan, V. Perrier, and K. Schneider. Turbulence analysis, modelling and computing using wavelets. In J. van den Berg, editor, *Wavelets in Physics*, chapter 4. Cambridge U. Press, 1999.

J. Fröhlich and M. Uhlmann. Orthonormal polynomial wavelets on the interval and applications to the analysis of turbulent flow fields. *(accepted for publication in SIAM J. Appl. Math.)*, 2002.

J. Fröhlich, M. Uhlmann, and J. Prestin. The construction of localized Legendre wavelets for the interval. *(in preparation)*, 2003.

J. Jeong, F. Hussain, W. Schoppa, and J. Kim. Coherent structures near the wall in a turbulent channel flow. *J. Fluid Mech.*, 332:185–214, 1997.

Z. Liu, R. Adrian, and T. Hanratty. Large-scale modes of turbulent channel flow: transport and structure. *J. Fluid Mech.*, 448:53–80, 2001.

Y. Maday and J. Ravel. Adaptativité par ondelettes: conditions aux limites et dimensions supérieures. *C.R. Acad. Sci. Paris, Série I*, 315:85–90, 1992.

S. Mallat. A theory for multiresolution signal decomposition: the wavelet representation. *IEEE Trans. Pattern Analysis Mach. Intell.*, 11(7):674–693, 1989.

H. Malvar. Lapped transforms for efficient transform / subband coding. *IEEE Trans. Acoust. Speech Signal Process.*, 38:969–978, 1990.

C. Meneveau. Analysis of turbulence in the orthonormal wavelet representation. *J. Fluid Mech.*, 232:469–520, 1991.

A. Townsend. *The Structure of Turbulent Shear Flow.* Cambridge U. Press, second edition, 1976.

M. Uhlmann and J. Fröhlich. Local spectra in plane channel flow using wavelets designed for the interval. In I. Castro, P. Hancock, and T. Thomas, editors, *Advances in Turbulence IX*, Proc. 9th Eur. Turb. Conf., pages 111–114, Southampton, UK, 2002.